

Phononic and electronic properties of the superconducting topological metal $\text{ThMo}_2\text{Si}_2\text{C}$

Xian-Biao Shi,^{1,2,*} Jing-Yu Li^{1,2,*}, Jian-Guo Si,³ Lan-Ting Shi,^{1,2} Peng-Fei Liu,^{1,2} and Bao-Tian Wang^{1,2,4,†}

¹*Institute of High Energy Physics, Chinese Academy of Sciences, Beijing 100049, China*

²*Spallation Neutron Source Science Center, Dongguan 523803, China*

³*Songshan Lake Materials Laboratory, Dongguan 523808, China*

⁴*Collaborative Innovation Center of Extreme Optics, Shanxi University, Taiyuan, Shanxi 030006, China*



(Received 9 January 2024; revised 2 July 2024; accepted 5 August 2024; published 13 August 2024)

The phononic and electronic properties of newly discovered quaternary superconductor $\text{ThMo}_2\text{Si}_2\text{C}$ are reported based on the results of first-principles calculations. The phonon spectrum contains soft phonon modes around the zone corners that lead to a $\sqrt{2} \times \sqrt{2} \times 1$ charge-density-wave (CDW) instability, which is related to the momentum-dependent electron-phonon coupling. Intriguingly, these soft phonon modes can be removed by considering anharmonic effects. The electronic band structure without spin-orbit coupling (SOC) hosts multiple band crossing points near the Fermi level (E_f), giving rise to multiple bulk nodal lines in this system. When SOC is considered, the nodal lines are gapped out and a pair of anisotropic Dirac points protected by C_4 rotational symmetry emerge along the Γ - Z direction near the E_f . These results suggest that superconductor $\text{ThMo}_2\text{Si}_2\text{C}$ is a topological Dirac metal on the verge of a CDW instability, making it a realistic material platform to investigate the interplay among superconductivity, CDW quantum criticality, and bulk Dirac fermions.

DOI: [10.1103/PhysRevB.110.075129](https://doi.org/10.1103/PhysRevB.110.075129)

I. INTRODUCTION

Layered titanium-based pnictide oxide superconductors $\text{BaTi}_2\text{Pn}_2\text{O}$ ($\text{Pn} = \text{Sb}, \text{Bi}$) that crystallize in tetragonal $\text{CeCr}_2\text{Si}_2\text{C}$ -type structure with anti- CuO_2 -type Ti_2O square lattice have been discovered to show highly diverse physical properties, including superconductivity, spin/charge density wave (S/CDW), and topologically nontrivial electronic band structure [1–14]. Especially, the coexistence of superconductivity and topological states in $\text{BaTi}_2\text{Pn}_2\text{O}$ makes them promising candidates for topological superconductors (TSCs) [13,14]. TSCs have attracted great research interest in the condensed matter physics community due to the emergence of Majorana fermions and the potential application in topological quantum computation [15–21]. Following the $\text{BaTi}_2\text{Pn}_2\text{O}$, various kinds of compounds with tetragonal $\text{CeCr}_2\text{Si}_2\text{C}$ -type structure, such as $\text{ATM}_2\text{Ch}_2\text{O}$ ($A = \text{K}, \text{Rb}, \text{Cs}$; $\text{TM} = \text{Ti}, \text{V}$; $\text{Ch} = \text{S}, \text{Se}, \text{Te}$) [22–26], $\text{BaFe}_2\text{Ch}_2\text{O}$ ($\text{Ch} = \text{S}, \text{Se}$) [27,28], and $\text{LaTM}_2\text{Al}_2\text{B}$ ($\text{TM} = \text{Ru}, \text{Os}$) [29,30], have been synthesized to search for new superconductors. However, none of these listed compounds exhibit any sign of superconductivity.

Recently, a new layered quaternary compound, $\text{ThMo}_2\text{Si}_2\text{C}$, has been synthesized by Liu *et al.* [31]. $\text{ThMo}_2\text{Si}_2\text{C}$ crystallizes in the same crystal structure as $\text{BaTi}_2\text{Pn}_2\text{O}$ and exhibits a superconducting transition at $T_c = 2.2$ K, which is higher than that of $\text{BaTi}_2\text{Sb}_2\text{O}$ ($T_c = 1.2$ K) [3,4] but lower than that of $\text{BaTi}_2\text{Bi}_2\text{O}$ ($T_c = 4.6$ K) [5]. Based on the measurements of magnetic susceptibility and electronic resistivity, Liu *et al.* found that S/CDW instability is absent in $\text{ThMo}_2\text{Si}_2\text{C}$. They thus suggested that the origin of superconductivity in $\text{ThMo}_2\text{Si}_2\text{C}$

is different from that in $\text{BaTi}_2\text{Pn}_2\text{O}$ [31]. The discovery of superconductivity in $\text{ThMo}_2\text{Si}_2\text{C}$ may open a new direction of searching for new superconductors in compounds crystallizing in tetragonal $\text{CeCr}_2\text{Si}_2\text{C}$ -type structure without the Ti_2O square lattice.

Studying the phononic and electronic properties is crucial for understanding the superconducting behaviors of newly discovered superconductors. Herein, we present our first-principles calculations of the phononic and electronic properties for $\text{ThMo}_2\text{Si}_2\text{C}$. The calculated phonon dispersions show that the undistorted $\text{ThMo}_2\text{Si}_2\text{C}$ is dynamically unstable with zone corner soft phonon modes and undergoes a $\sqrt{2} \times \sqrt{2} \times 1$ structural reconstruction to form an energetically favored CDW state. By calculating the Fermi surface nesting function and analyzing the momentum-dependent linewidth of the lowest phonon mode, we propose that the electron-phonon coupling (EPC) plays a significant role in driving CDW instability. The calculated electronic band structure shows that $\text{ThMo}_2\text{Si}_2\text{C}$ is a topological metal, hosting multiple nodal lines near the E_f in the absence of spin-orbit coupling (SOC). In the presence of SOC, the nodal lines are destroyed and a pair of anisotropic Dirac points emerge along the Γ - Z direction located at the Brillouin zone (BZ) coordinates $(0, 0, k_z^D \approx \pm 0.328 \times \frac{2\pi}{c})$, about $E_D = 56$ meV above the E_f . These results not only provide useful information for understanding the superconducting behaviors in $\text{ThMo}_2\text{Si}_2\text{C}$ but also make it more attractive.

II. METHODS

Our first-principles calculations were performed using the projector augmented wave (PAW) method [32,33] and selected the generalized gradient approximation (GGA) [34] with Perdew-Burke-Ernzerhof (PBE) type [35], as encoded

*These authors contributed equally to this work.

†Contact author: wangbt@ihep.ac.cn

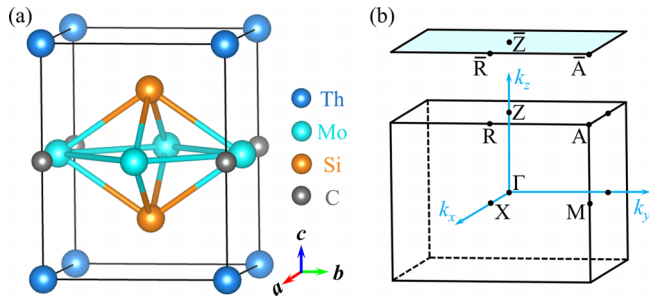


FIG. 1. (a) Crystal structure of $\text{ThMo}_2\text{Si}_2\text{C}$. (b) Bulk BZ and its projection onto the (001) surface.

in the Vienna *Ab initio* Simulation Package (VASP) [36–38]. A kinetic energy cutoff of 500 eV and a Γ -centred k -point mesh of $12 \times 12 \times 10$ were utilized for all electronic structure calculations. During self-consistent convergence and structural relaxation, the energy and force difference criteria were defined as 10^{-6} eV and 0.01 eV/Å. The irreducible representations were obtained by the program IRVSP [39]. The WANNIER90 package [40–42] was employed to construct the Wannier functions from the first-principles results. Topological properties calculations were carried out by using the WANNIERTOOLS code [43].

For phonon dispersions calculations, the density functional perturbation theory (DFPT) [44] as implemented in the QUANTUM ESPRESSO package [45] was utilized, with GGA potentials. The cutoff energies of the wave functions and charge density were set as 100 and 1000 Ry, respectively. The Gaussian smearing method was used to calculate the charge density with a smearing parameter of $\sigma = 0.01$ Ry. During self-consistent calculations, Γ -centered k -point meshes of $16 \times 16 \times 12$ and $12 \times 12 \times 12$ were utilized for undistorted and distorted structures, respectively. For the dynamical matrix calculations, $8 \times 8 \times 6$ and $6 \times 6 \times 6$ \mathbf{q} -point meshes were adopted for the undistorted and distorted structures, respectively. The DynaPhoPy code [46] was used to calculate the anharmonic lattice dynamics from the *ab initio* molecular dynamics simulations.

III. RESULTS AND DISCUSSION

The $\text{ThMo}_2\text{Si}_2\text{C}$ investigated here crystallizes in a tetragonal $\text{CeCr}_2\text{Si}_2\text{C}$ -type structure with space group $P4/mmm$ (No. 123) [31], as shown in Fig. 1(a). It is composed of $\text{Mo}_2\text{Si}_2\text{C}$ layers and Th atomic layers, alternatively appearing along the c direction. In the $\text{Mo}_2\text{Si}_2\text{C}$ layer, the Mo atom is twofold coordinated with C atoms, creating a planar Mo_2C sheet with a checkerboard pattern. The experimentally determined lattice constants and internal atomic coordinate are $a = b = 4.22963$ Å, $c = 5.35714$ Å, and $z_{\text{Si}} = 0.22676$ [31]. After fully structural optimization, we obtain $a = b = 4.23996$ Å, $c = 5.36614$ Å, and $z_{\text{Si}} = 0.22093$, in excellent agreement with the experimental values. These fully optimized structural parameters are adopted in the following calculations. The bulk BZ, projected (001) surface BZ, and high-symmetry points are shown in Fig. 1(b).

Previous studies on $\text{BaTi}_2\text{Pn}_2\text{O}$ indicate that the phonon spectrum contains valuable information regarding dynamical

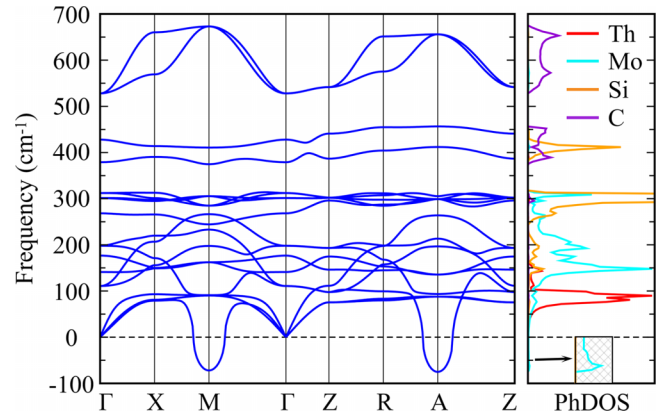


FIG. 2. Calculated harmonic phonon dispersions (left panel) and projected PhDOS (right panel) for undistorted $\text{ThMo}_2\text{Si}_2\text{C}$. The negative frequency means the imaginary value of the softened phonon frequency.

stability, CDW, and superconductivity [11,12]. We thus first calculate the phononic band structure for $\text{ThMo}_2\text{Si}_2\text{C}$ in the undistorted tetragonal structure based on the fully relaxed lattice parameters. The resulting phonon dispersion curves along the high-symmetry lines of the BZ are presented in the left panel of Fig. 2. A conspicuous feature of the phonon spectrum is the appearance of phonon softening instabilities around M ($\frac{1}{2}, \frac{1}{2}, 0$) and A ($\frac{1}{2}, \frac{1}{2}, \frac{1}{2}$) high-symmetry points, clearly indicating the dynamical instability of undistorted $\text{ThMo}_2\text{Si}_2\text{C}$. This feature is rather similar to the situation observed in $\text{BaTi}_2\text{Pn}_2\text{O}$ [11,12]. The projected phonon density of states (PhDOS) in the right panel of Fig. 2 shows that the soft phonon modes have only Mo character, emphasizing that the Mo square sheet is unstable. By analyzing the eigenvectors of the soft phonon modes, the motion of Mo atoms can be distinguished. A schematic illustration of the eigenvectors for the soft phonon modes is shown in Fig. 3(a), where the arrows indicate the directions of the atomic vibrations. It can be seen that the soft phonon modes correspond to the displacement mode of all Mo ions moving perpendicular to the Mo-C nearest-neighbor bonds.

Phonon softening has been widely discussed in terms of CDW instability [47–49]; it is thus natural to examine whether the CDW instability is present in $\text{ThMo}_2\text{Si}_2\text{C}$. To address this point, we construct a series of $\sqrt{2} \times \sqrt{2} \times 1$ supercells with the unit cell axes rotated by 45° and perform a frozen phonon analysis by displacing Mo atoms according to the eigenvectors of the soft phonon modes, as shown in Fig. 3(b). The relative energies of these supercells with respect to the undistorted structure as a function of the amplitude of the Mo atomic displacement are plotted in Fig. 3(c). The results show that the undistorted structure is energetically unfavorable and the energy exhibits a minimal at a finite value of the atomic displacement. The calculated total energy per formula unit is lower by 0.157 meV for the distorted structure relative to the undistorted structure. The magnitude of the atomic displacements which minimizes the total energy is 0.0375 Å. Figure 3(d) shows the phonon spectrum of the energetically favored structure obtained by displacing atoms along the soft mode eigenvectors. As expected, the soft phonon

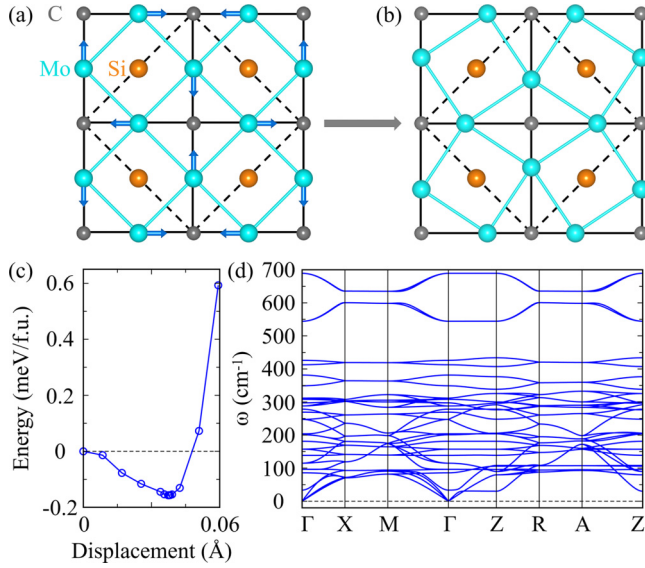


FIG. 3. Top view of Mo₂Si₂C layer in the (a) undistorted structure and (b) distorted structure. Arrows in (a) represent the atomic vibrational patterns corresponding to the soft phonon modes in Fig. 2. Solid lines indicate the primitive unit cell, while dashed lines denote the $\sqrt{2} \times \sqrt{2} \times 1$ supercell. (c) Total energy variation of the $\sqrt{2} \times \sqrt{2} \times 1$ supercell with respect to the displacement of Mo atoms. Energies are given relative to the undistorted structure energy. (d) Calculated phonon dispersions for distorted ThMo₂Si₂C.

modes vanish, reflecting the dynamical stability of this distorted structure.

Based on the results above, we hence propose that the soft phonon modes in the phonon spectrum give rise to a CDW instability in ThMo₂Si₂C with similar distortion pattern as in the BaTi₂Pn₂O cases [11,12]. According to the formation mechanism of CDW, Zhu *et al.* [50] suggested that there are at least three types of CDWs. Type-I CDWs are quasi-1D systems with their origin in Fermi surface nesting. Type-II CDWs are driven by EPC but not by Fermi surface nesting. Other CDWs belong to type III. To identify the origin of the CDW instability in ThMo₂Si₂C, we calculate the Fermi surface nesting function and the EPC for undistorted ThMo₂Si₂C.

Figure 4 shows the calculated electronic band structure and Fermi surface sheets. There are three bands crossing the E_f , forming three Fermi surface sheets. The first sheet is a corrugated quasi-two-dimensional cylindrical sheet located around the corners of the BZ. The second and third sheets have a three-dimensional character. Using the calculated Fermi surface in Fig. 4(b), we calculate the Fermi surface nesting function $\xi(\mathbf{q}) = \sum_{k,m,n,v} \delta(\varepsilon_{k,n} - \varepsilon_F) \delta(\varepsilon_{k+q,m} - \varepsilon_F)$, where δ is the Dirac-delta function, $\varepsilon_{k,n}$ is the eigenvalue of band n at \mathbf{k} , ε_F is the Fermi energy, and \mathbf{q} is the nesting vector. This function is the imaginary part of the electronic susceptibilities [51]. The results are shown in Fig. 5(a). Since the phononic band structure shows soft phonon modes around M and A points, the nesting functions thus should have pronounced maximum value at the M and A points on the $k_z = 0$ plane and the $k_z = 0.5$ plane, respectively, if the Fermi surface nesting is the origin of the formation of the CDW instability [51,52]. This is obviously not what is seen in Fig. 5(a). Thus the Fermi

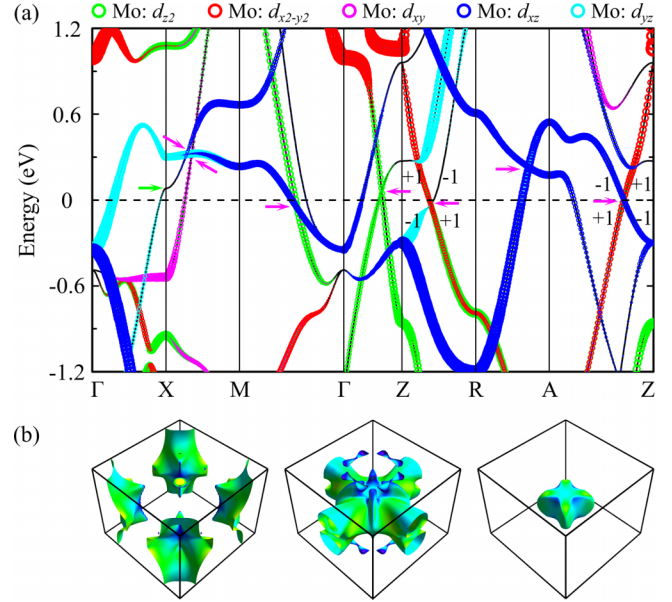


FIG. 4. (a) Calculated orbital-resolved electronic band structure for undistorted ThMo₂Si₂C without SOC inclusion. Magenta arrows mark the multiple BCPs, the van Hove singularity at X high-symmetry point is marked with green arrow. ± 1 denote the eigenvalues of the mirror symmetry M_z . (b) The corresponding Fermi surface; each band is shown separately.

surface nesting effect cannot be responsible for the CDW formation in ThMo₂Si₂C.

In Fig. 5(b), the phonon linewidth γ of the lowest phonon mode for undistorted ThMo₂Si₂C on the $k_z = 0$ plane and the $k_z = 0.5$ plane is plotted. The phonon linewidth γ is

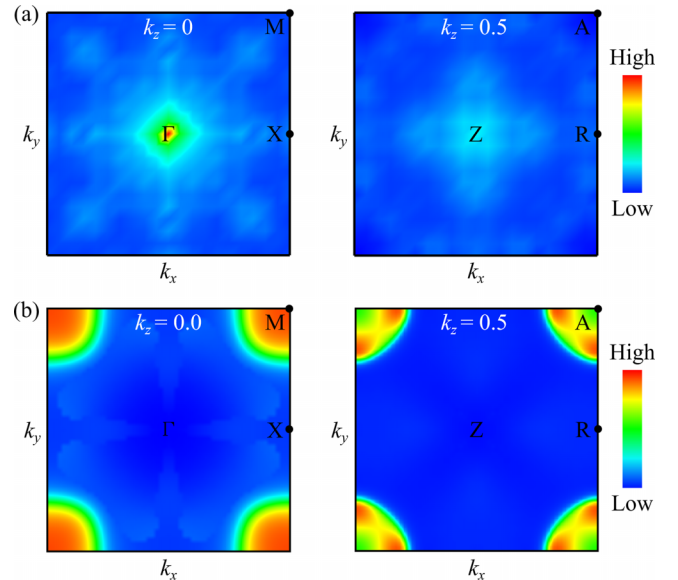


FIG. 5. (a) Calculated Fermi surface nesting function for undistorted ThMo₂Si₂C on the (left) $k_z = 0$ plane and the (right) $k_z = 0.5$ plane. (b) Calculated phonon linewidth γ of the lowest phonon mode for undistorted ThMo₂Si₂C on the (left) $k_z = 0$ plane and the (right) $k_z = 0.5$ plane.

defined as

$$\gamma_{qv} = 2\pi\omega_{qv} \sum_{ij} \int \frac{d^3\mathbf{k}}{\Omega_{BZ}} |g_{qv}(\mathbf{k}, i, j)|^2 \times \delta(\varepsilon_{q,i} - \varepsilon_F) \delta(\varepsilon_{k+q,j} - \varepsilon_F). \quad (1)$$

Here, ω_{qv} is the phonon frequency, Ω_{BZ} is the volume of the first BZ, $\varepsilon_{q,i}$ is the energy of band i with wave number q , ε_F is the Fermi level, and $g_{qv}(\mathbf{k}, i, j)$ is the electron-phonon coefficient and can be obtained by

$$g_{qv}(\mathbf{k}, i, j) = \left(\frac{\hbar}{2M\omega_{qv}} \right)^{1/2} \langle \psi_{i,\mathbf{k}} | \frac{dV_{\text{SCF}}}{d\hat{u}_{qv}} \cdot \hat{\varepsilon}_{qv} | \psi_{j,\mathbf{k}+\mathbf{q}} \rangle, \quad (2)$$

where ψ is the wave function, V_{SCF} is the Kohn-Sham potential, \hat{u} is the atomic displacement, and $\hat{\varepsilon}$ is the phonon eigenvector. From the definition above, we can know that the phonon linewidth γ is directly related to the strength of the EPC [53–57]. On the $k_z = 0$ and $k_z = 0.5$ planes, we can see that the phonon linewidth γ in Fig. 5(b) shows broad peaks at the M and A points, respectively. This indicates that the EPC plays a critical role in driving CDW instability in $\text{ThMo}_2\text{Si}_2\text{C}$, similar to the situation in $\text{BaTi}_2\text{Sb}_2\text{O}$ [11].

Besides the Fermi surface nesting and EPC mechanisms, the Van Hove singularity [58] and excitonic insulator [59,60] are also considered important mechanisms leading to CDW instability. However, for $\text{ThMo}_2\text{Si}_2\text{C}$, the calculated electronic band structure shows multiple bands crossing the E_f , indicating metallic properties. Therefore, we can exclude the excitonic insulator mechanism, as this mechanism is applicable to semimetallic or semiconductor systems. Additionally, from the band structure of $\text{ThMo}_2\text{Si}_2\text{C}$, it can be observed that there is a Van Hove singularity at the X high-symmetry point, as indicated by the green arrow in Fig. 4(a), but it is located above the E_f . Consequently, it is also unlikely to induce a CDW phase transition in $\text{ThMo}_2\text{Si}_2\text{C}$.

As such, at the DFT level, $\text{ThMo}_2\text{Si}_2\text{C}$ favors a CDW ground state, which is related to the EPC. However, this is in contrast to available experiments, which show that no CDW-like anomaly is observed in the electrical resistivity and magnetic susceptibility of $\text{ThMo}_2\text{Si}_2\text{C}$ [31]. Such a discrepancy between theoretically predicted CDW instability and experimentally unobserved anomalies is similar to the situation that occurred in $2H\text{-NbS}_2$ [61,62], $\text{LaO}_{0.5}\text{F}_{0.5}\text{BiS}_2$ [63,64], and $\text{BaTi}_2\text{Bi}_2\text{O}$ [12] superconductors. It is noteworthy that the energy scale of the predicted CDW instability is only 0.026 meV/atom. This indicates that the structure can be stabilized by anharmonic effects, as observed in $2H\text{-NbS}_2$ [61,62]. To unveil the crucial role of anharmonic effects in $\text{ThMo}_2\text{Si}_2\text{C}$, we present its anharmonic phonon spectra and projected PhDOS in Fig. 6. It is evident that the anharmonic effects remove the lattice instabilities at the harmonic level. It is thus safe to draw the conclusion that $\text{ThMo}_2\text{Si}_2\text{C}$ is on the verge of a CDW instability.

We now move to the electronic properties of $\text{ThMo}_2\text{Si}_2\text{C}$. Since $\text{ThMo}_2\text{Si}_2\text{C}$ resides near the CDW phase rather than undergoing a CDW phase transition, its electronic properties are hence still determined by the normal state. We thus primarily investigate the electronic structure and topological properties of $\text{ThMo}_2\text{Si}_2\text{C}$ in its undistorted structure here. The

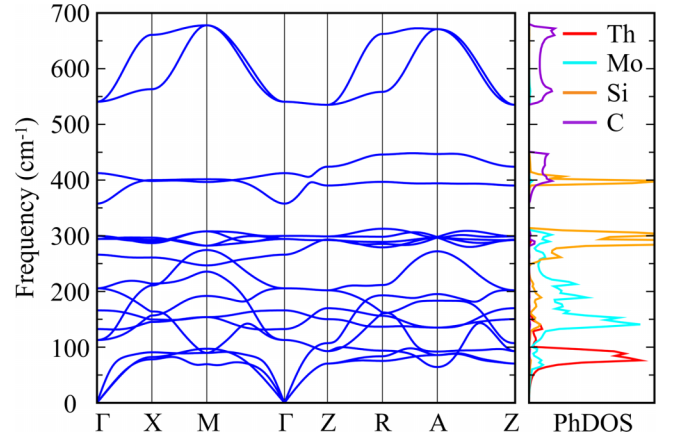


FIG. 6. Calculated anharmonic phonon dispersions (left panel) and projected PhDOS (right panel) for undistorted $\text{ThMo}_2\text{Si}_2\text{C}$.

electronic band structure of $\text{ThMo}_2\text{Si}_2\text{C}$ without SOC is shown in Fig. 4(a), in which the different colors denote the orbital characters. It unveils a metallic ground state with both electron and hole Fermi surface sheets [see Fig. 4(b)]. The marked feature in the electronic band structure of $\text{ThMo}_2\text{Si}_2\text{C}$ is the presence of multiple fascinating band crossing points (BCPs) near the E_f , as indicated by the magenta arrows. Further analysis of orbital characters shows that these BCPs are primarily dominated by Mo-4d orbitals. Because of the presence of both time-reversal \mathcal{T} and inversion \mathcal{P} symmetries, the BCPs in $\text{ThMo}_2\text{Si}_2\text{C}$ cannot be isolated [65]. After a careful inspection of BCPs in full bulk BZ, we find that these BCPs in fact form multiple nodal lines, as shown in Fig. 7(a). Among all the nodal lines, the nodal ring on the $k_z = 0.5$ plane is closest to the E_f . Besides, this nodal ring is quite flat with an energy variation less than 0.1 eV, as shown in Fig. 7(c). It should be emphasized that this nodal ring is protected by two sets of symmetries: (a) the combination of \mathcal{T} and \mathcal{P}

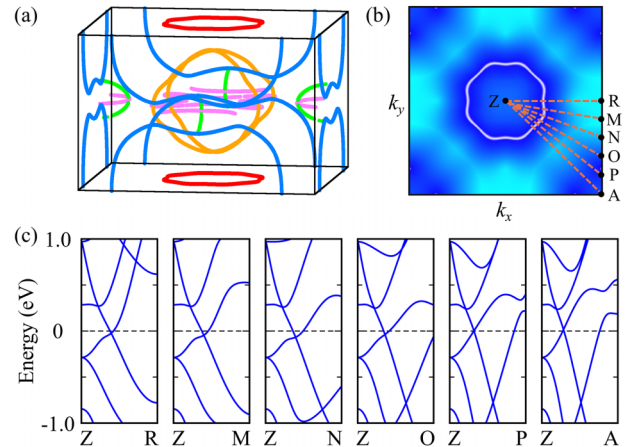


FIG. 7. (a) Distribution of the BCPs in the first bulk BZ. Multiple nodal lines are observed, which are colored by orchid, red, orange, green, and web blue, respectively. (b) The shape of nodal ring centered at Z point on the $k_z = 0.5$ plane and the selected k paths through the nodal ring. (c) Band structure on the $k_z = 0.5$ plane along selected directions, which are marked in (b).

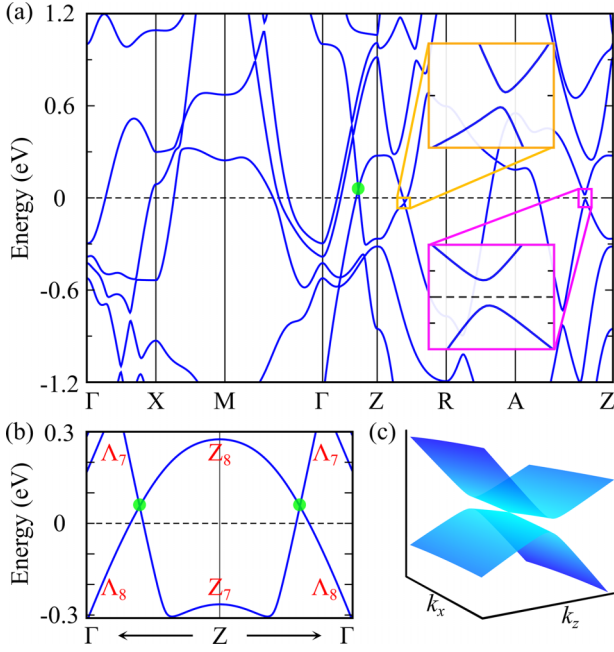


FIG. 8. (a) Calculated electronic band structure for undistorted $\text{ThMo}_2\text{Si}_2\text{C}$ with SOC inclusion. The insets show a zoom in band structure around Z point. (b) Energy dispersion along the Γ -Z line displaying a pair of Dirac points. The irreducible representations of selected bands are indicated. (c) Three-dimensional band structure on the k_x - k_z plane around the Dirac point.

symmetries in the absence of SOC, and (b) the mirror symmetry M_z . The reason why this nodal ring is also protected by the M_z symmetry is that the two crossing bands within this mirror invariant plane belong to two opposite mirror eigenvalues ± 1 , as shown in Fig. 4(a).

To delineate the SOC effect on the electronic structure of $\text{ThMo}_2\text{Si}_2\text{C}$, we plot the electronic band structure with SOC in Fig. 8(a). Upon including SOC, we find that nearly all the BCPs are gapped, except for the BCP along the Γ -Z line, as indicated by the green dot in Fig. 8(a). Along the Γ -Z line, the little group is C_{4v} for any k point. Symmetry analysis shows that the crossing bands belong to different irreducible representations, Λ_7 and Λ_8 , as shown in Fig. 8(b). The BCP along the Γ -Z line is thus unavoidable and protected by the C_4 rotational symmetry. Owing to the coexistence of \mathcal{T} and \mathcal{P} symmetries, every band is spin doubly degenerate. Hence, the BCP is fourfold degenerate, or, namely, a Dirac point. According to our calculations, the Dirac point is located at BZ coordinates $(0, 0, k_z^D \approx \pm 0.328 \times \frac{2\pi}{c})$ with an energy of $E_D = 56 \text{ meV}$ above the E_f . It is worth emphasizing that the Dirac cone is anisotropic because it has different slopes along the in-plane and out-of-plane directions, as supported by the three-dimensional band structure around the Dirac point in Fig. 8(c).

Our electronic structure calculations indicate that superconductor $\text{ThMo}_2\text{Si}_2\text{C}$ is a topological metal with symmetry-protected Dirac points near the E_f . To further confirm the topologically nontrivial nature of $\text{ThMo}_2\text{Si}_2\text{C}$, we calculate the Fu-Kane \mathbb{Z}_2 topological invariant from the parities of

TABLE I. The products of parity eigenvalues of the occupied states for TRIM points Γ , X , M , A , Z , and R in the BZ.

Γ	$X (\times 2)$	M	A	Z	$R (\times 2)$
-	-	+	-	+	-

all occupied bands at the time-reversal invariant momentum (TRIM) points [66]. Table I shows the product of the parity eigenvalues of the occupied bands at the eight TRIM points. According to our calculations, $\text{ThMo}_2\text{Si}_2\text{C}$ is a three-dimensional weak topological metal, with 3D \mathbb{Z}_2 invariants given by $(0; 111)$. Topological metals hosting symmetry-protected Dirac points with a weak \mathbb{Z}_2 topological invariant have been reported in Pt_3Sn [67] and YTi_3 [68]. A single material containing both superconductivity and bulk Dirac points has been theoretically suggested as a promising platform for the realization of a superconducting Dirac semimetal, in which the interaction between bulk Dirac points and superconductivity can sustain an exotic quasiparticle excitation, namely, a gapless one-dimensional helical Majorana mode [68–74]. Therefore, the coexistence of superconductivity and bulk Dirac fermions in $\text{ThMo}_2\text{Si}_2\text{C}$ suggests that it could be a realistic material for future studies of helical Majorana fermions.

IV. CONCLUSION

In conclusion, on the basis of first-principles calculations, we have studied the phononic and electronic properties of the newly discovered superconductor $\text{ThMo}_2\text{Si}_2\text{C}$. We find that this superconductor shows an unexpected CDW instability. The formation of the CDW is mainly caused by the inhomogeneous distribution of the EPC. The appearance of CDW is in disagreement with available experimental measurements. We thus conclude that $\text{ThMo}_2\text{Si}_2\text{C}$ is actually on the verge of a CDW instability. We also predict that this superconductor is a topological metal. There are multiple type-I and type-II BCPs in the electronic band structure without SOC. The BCPs form multiple bulk nodal lines in this system. When SOC is included, the nodal lines are destroyed and a pair of anisotropic Dirac points emerge along the Γ -Z direction. These results suggest that $\text{ThMo}_2\text{Si}_2\text{C}$ would provide a realistic material platform for studying intriguing properties arising from the interplay of superconductivity, CDW quantum criticality, and band topology.

ACKNOWLEDGMENTS

The authors gratefully acknowledge financial support from the National Natural Science Foundation of China (Grants No. 12074381, No. U2330104, and No. 12304095) and the Guangdong Basic and Applied Basic Research Foundation (Grants No. 2023A1515110410, No. 2024A1515010484, and No. 2023A1515111190). The calculations were performed at the CSNS Scientific Computing Platform of the Institute of High Energy Physics of CAS and the GBA Sub-Center of the National HEP Science Data Center.

- [1] B. Lorenz, A. M. Guloy, and P. C. W. Chu, Superconductivity in titanium-based pnictide oxide compounds, *Int. J. Mod. Phys. B* **28**, 1430011 (2014).
- [2] T. Yajima, Titanium pnictide oxide superconductors, *Condens. Matter* **2**, 4 (2017).
- [3] P. Doan, M. Gooch, Z. Tang, B. Lorenz, A. Möller, P. C. W. Chu, and A. M. Guloy, $\text{Ba}_{1-x}\text{Na}_x\text{Ti}_2\text{Sb}_2\text{O}$ ($0.0 \leq x \leq 0.33$): A layered titanium-based pnictide oxide superconductor, *J. Am. Chem. Soc.* **134**, 16520 (2012).
- [4] T. Yajima, K. Nakano, F. Takeiri, T. Ono, Y. Hosokoshi, Y. Matsushita, J. Heister, Y. Kobayashi, and H. Kageyama, Superconductivity in $\text{BaTi}_2\text{Sb}_2\text{O}$ with a d^1 square lattice, *J. Phys. Soc. Jpn.* **81**, 103706 (2012).
- [5] T. Yajima, K. Nakano, F. Takeiri, J. Hester, T. Yamamoto, Y. Kobayashi, N. Tsuji, J. Kim, A. Fujiwara, and H. Kageyama, Synthesis and physical properties of the new oxybismuthides $\text{BaTi}_2\text{Bi}_2\text{O}$ and $(\text{SrF})_2\text{Ti}_2\text{Bi}_2\text{O}$ with a d^1 square net, *J. Phys. Soc. Jpn.* **82**, 013703 (2013).
- [6] T. Yajima, K. Nakano, F. Takeiri, Y. Nozaki, Y. Kobayashi, and H. Kageyama, Two superconducting phases in the isovalent solid solutions $\text{BaTi}_2\text{Pn}_2\text{O}$ ($\text{Pn} = \text{As, Sb, and Bi}$), *J. Phys. Soc. Jpn.* **82**, 033705 (2013).
- [7] H.-F. Zhai, W.-H. Jiao, Y.-L. Sun, J.-K. Bao, H. Jiang, X.-J. Yang, Z.-T. Tang, Q. Tao, X.-F. Xu, Y.-K. Li, C. Cao, J.-H. Dai, Z.-A. Xu, and G.-H. Cao, Superconductivity, charge- or spin-density wave, and metal-nonmetal transition in $\text{BaTi}_2(\text{Sb}_{1-x}\text{Bi}_x)_2\text{O}$, *Phys. Rev. B* **87**, 100502(R) (2013).
- [8] F. von Rohr, A. Schilling, R. Nesper, C. Baines, and M. Bendele, Conventional superconductivity and charge-density-wave ordering in $\text{Ba}_{1-x}\text{Na}_x\text{Ti}_2\text{Sb}_2\text{O}$, *Phys. Rev. B* **88**, 140501(R) (2013).
- [9] S. Kamusella, P. Doan, T. Goltz, H. Luetkens, R. Sarkar, A. Guloy, and H.-H. Klauss, CDW order and unconventional s -wave superconductivity in $\text{Ba}_{1-x}\text{Na}_x\text{Ti}_2\text{Sb}_2\text{O}$, *J. Phys.: Conf. Ser.* **551**, 012026 (2014).
- [10] Q. Song, Y. J. Yan, Z. R. Ye, M. Q. Ren, D. F. Xu, S. Y. Tan, X. H. Niu, B. P. Xie, T. Zhang, R. Peng, H. C. Xu, J. Jiang, and D. L. Feng, Electronic structure of the titanium-based oxypnictide superconductor $\text{Ba}_{0.95}\text{Na}_{0.05}\text{Ti}_2\text{Sb}_2\text{O}$ and direct observation of its charge density wave order, *Phys. Rev. B* **93**, 024508 (2016).
- [11] A. Subedi, Electron-phonon superconductivity and charge density wave instability in the layered titanium-based pnictide $\text{BaTi}_2\text{Sb}_2\text{O}$, *Phys. Rev. B* **87**, 054506 (2013).
- [12] K. Nakano, K. Hongo, and R. Maezono, Phonon dispersions and Fermi surfaces nesting explaining the variety of charge ordering in titanium-oxypnictides superconductors, *Sci. Rep.* **6**, 29661 (2016).
- [13] X. Shi, L. Chen, P. He, G. Wang, G. Zheng, X. Liu, and W. Zhao, Dirac fermions in the layered titanium-based oxypnictide superconductor $\text{BaTi}_2\text{Bi}_2\text{O}$, *Phys. Rev. B* **99**, 155155 (2019).
- [14] Z. Huang, W. L. Liu, H. Y. Wang, Y. L. Su, Z. T. Liu, X. B. Shi, S. Y. Gao, Z. Y. Chen, Y. J. Yan, Z. C. Jiang, Z. H. Liu, J. S. Liu, X. L. Lu, Y. C. Yang, R. X. Zhou, W. Xia, Y. B. Huang, S. Qiao, W. W. Zhao, Y. F. Guo, G. Li, and D. W. Shen, Dual topological states in the layered titanium-based oxypnictide superconductor $\text{BaTi}_2\text{Sb}_2\text{O}$, *npj Quantum Mater.* **7**, 70 (2022).
- [15] S. R. Elliott and M. Franz, Colloquium: Majorana fermions in nuclear, particle, and solid-state physics, *Rev. Mod. Phys.* **87**, 137 (2015).
- [16] M. Sato and S. Fujimoto, Majorana fermions and topology in superconductors, *J. Phys. Soc. Jpn.* **85**, 072001 (2016).
- [17] M. Sato and Y. Ando, Topological superconductors: A review, *Rep. Prog. Phys.* **80**, 076501 (2017).
- [18] N. Hao and J. Hu, Topological quantum states of matter in iron-based superconductors: From concept to material realization, *Natl. Sci. Rev.* **6**, 213 (2019).
- [19] K. Flensberg, F. von Oppen, and A. Stern, Engineered platforms for topological superconductivity and Majorana zero modes, *Nat. Rev. Mater.* **6**, 944 (2021).
- [20] P.-F. Liu, J. Li, X.-H. Tu, H. Yin, B. Sa, J. Zhang, D. J. Singh, and B.-T. Wang, Prediction of superconductivity and topological aspects in single-layer β - Bi_2Pd , *Phys. Rev. B* **102**, 155406 (2020).
- [21] W. Qin, J. Gao, P. Cui, and Z. Zhang, Two-dimensional superconductors with intrinsic p -wave pairing or nontrivial band topology, *Sci. China Phys. Mech. Astron.* **66**, 267005 (2023).
- [22] M. Valldor, P. Merz, Y. Prots, and W. Schnelle, Bad-metal-layered sulfide oxide $\text{CsV}_2\text{S}_2\text{O}$, *Eur. J. Inorg. Chem.* **2016**, 23 (2016).
- [23] M. Valldor, P. Merz, Y. Prots, Y. Watier, and W. Schnelle, Synthesis and characterization of $\text{Cs}_{1-x}\text{Ti}_2\text{Te}_2\text{O}$ ($x \approx 0.2$): Electron doping by Te resulting in a layered metal, *Inorg. Chem.* **55**, 11337 (2016).
- [24] A. Ablimit, Y.-L. Sun, H. Jiang, S.-Q. Wu, Y.-B. Liu, and G.-H. Cao, Weak metal-metal transition in the vanadium oxytelluride $\text{Rb}_{1-\delta}\text{V}_2\text{Te}_2\text{O}$, *Phys. Rev. B* **97**, 214517 (2018).
- [25] H. Lin, J. Si, X. Zhu, K. Cai, H. Li, L. Kong, X. Yu, and H.-H. Wen, Structure and physical properties of $\text{CsV}_2\text{Se}_{2-x}\text{O}$ and $\text{V}_2\text{Se}_2\text{O}$, *Phys. Rev. B* **98**, 075132 (2018).
- [26] N. D. Kelly and S. J. Clarke, Structure and compositional trends in alkali-metal containing titanium and vanadium oxide chalcogenides and the new van der Waals phase $\text{Ti}_2\text{Te}_2\text{O}$, *J. Solid State Chem.* **327**, 124276 (2023).
- [27] F. Takeiri, Y. Matsumoto, T. Yamamoto, N. Hayashi, Z. Li, T. Tohyama, C. Tassel, C. Ritter, Y. Narumi, M. Hagiwara, and H. Kageyama, High-pressure synthesis of the layered iron oxyselenide $\text{BaFe}_2\text{Se}_2\text{O}$ with strong magnetic anisotropy, *Phys. Rev. B* **94**, 184426 (2016).
- [28] S.-J. Song, Y.-Q. Lin, B.-Z. Li, S.-Q. Wu, Q.-Q. Zhu, Z. Ren, and G.-H. Cao, Tetragonal polymorph of $\text{BaFe}_2\text{S}_2\text{O}$ as an antiferromagnetic Mott insulator, *Phys. Rev. Mater.* **6**, 055002 (2022).
- [29] J. V. Zaikina, Y.-J. Jo, and S. E. Lattner, Ruthenium intermetallics grown from La-Ni flux: Synthesis, structure, and physical properties, *Inorg. Chem.* **49**, 2773 (2010).
- [30] D. E. Bugaris, F. Han, J. Im, D. Y. Chung, A. J. Freeman, and M. G. Kanatzidis, Crystal growth, structures, and properties of the complex borides, $\text{LaOs}_2\text{Al}_2\text{B}$ and $\text{La}_2\text{Os}_2\text{AlB}_2$, *Inorg. Chem.* **54**, 8049 (2015).
- [31] Z. C. Liu, B. Z. Li, Y. S. Xiao, Q. C. Duan, Y. W. Cui, Y. X. Mei, Q. Tao, S. L. Wei, S. G. Tan, Q. Jing, Q. Lu, Y. P. Sun, Y. Y. Liu, S. G. Fu, H. Jiang, Z. Ren, Z. A. Xu, C. Wang, and G. H. Cao, Superconductivity in $\text{ThMo}_2\text{Si}_2\text{C}$ with Mo_2C square net, *Sci. China Phys. Mech. Astron.* **64**, 277411 (2021).
- [32] P. E. Blöchl, Projector augmented-wave method, *Phys. Rev. B* **50**, 17953 (1994).
- [33] J. Lehtomäki, I. Makkonen, M. A. Caro, A. Harju, and O. Lopez-Acevedo, Orbital-free density functional theory

- implementation with the projector augmented-wave method, *J. Chem. Phys.* **141**, 234102 (2014).
- [34] J. P. Perdew and Y. Wang, Accurate and simple analytic representation of the electron-gas correlation energy, *Phys. Rev. B* **45**, 13244 (1992).
- [35] J. P. Perdew, K. Burke, and M. Ernzerhof, Generalized gradient approximation made simple, *Phys. Rev. Lett.* **77**, 3865 (1996).
- [36] G. Kresse and J. Hafner, *Ab initio* molecular dynamics for liquid metals, *Phys. Rev. B* **47**, 558 (1993).
- [37] G. Kresse and J. Furthmüller, Efficiency of *ab-initio* total energy calculations for metals and semiconductors using a plane-wave basis set, *Comput. Mater. Sci.* **6**, 15 (1996).
- [38] G. Kresse and J. Furthmüller, Efficient iterative schemes for *ab initio* total-energy calculations using a plane-wave basis set, *Phys. Rev. B* **54**, 11169 (1996).
- [39] J. Gao, Q. Wu, C. Persson, and Z. Wang, Irvsp: To obtain irreducible representations of electronic states in the VASP, *Comput. Phys. Commun.* **261**, 107760 (2021).
- [40] A. A. Mostofi, J. R. Yates, Y.-S. Lee, I. Souza, D. Vanderbilt and N. Marzari, wannier90: A tool for obtaining maximally-localised Wannier functions, *Comput. Phys. Commun.* **178**, 685 (2008).
- [41] N. Marzari and D. Vanderbilt, Maximally localized generalized Wannier functions for composite energy bands, *Phys. Rev. B* **56**, 12847 (1997).
- [42] I. Souza, N. Marzari, and D. Vanderbilt, Maximally localized Wannier functions for entangled energy bands, *Phys. Rev. B* **65**, 035109 (2001).
- [43] Q. S. Wu, S. N. Zhang, H. F. Song, M. Troyer, and A. A. Soluyanov, WannierTools: An open-source software package for novel topological materials, *Comput. Phys. Commun.* **224**, 405 (2018).
- [44] S. Baroni, S. de Gironcoli, A. Dal Corso, and P. Giannozzi, Phonons and related crystal properties from density-functional perturbation theory, *Rev. Mod. Phys.* **73**, 515 (2001).
- [45] P. Giannozzi, S. Baroni, N. Bonini, M. Calandra, R. Car, C. Cavazzoni, D. Ceresoli, G. L. Chiarotti, M. Cococcioni, I. Dabo *et al.*, QUANTUM ESPRESSO: A modular and open-source software project for quantum simulations of materials, *J. Phys.: Condens. Matter* **21**, 395502 (2009).
- [46] A. Carreras, A. Togo, and I. Tanaka, DynaPhoPy: A code for extracting phonon quasiparticles from molecular dynamics simulations, *Comput. Phys. Commun.* **221**, 221 (2017).
- [47] Z. Xu, H. Yang, X. Song, Y. Chen, H. Yang, M. Liu, Z. Huang, Q. Zhang, J. Sun, L. Liu and Y. Wang, Topical review: Recent progress of charge density waves in 2D transition metal dichalcogenide-based heterojunctions and their applications, *Nanotechnology* **32**, 492001 (2021).
- [48] C. Jiang, E. Beneduce, M. Baggioli, C. Setty, and A. Zaccane, Possible enhancement of the superconducting due to sharp Kohn-like soft phonon anomalies, *J. Phys.: Condens. Matter* **35**, 164003 (2023).
- [49] B.-T. Wang, P.-F. Liu, J.-J. Zheng, W. Yin, and F. Wang, First-principles study of superconductivity in the two- and three-dimensional forms of PbTiSe₂: Suppressed charge density wave in 1T-TiSe₂, *Phys. Rev. B* **98**, 014514 (2018).
- [50] X. Zhu, Y. Cao, J. Zhang, E. W. Plummer, and J. Guo, Classification of charge density waves based on their nature, *Proc. Natl. Acad. Sci. USA* **112**, 2367 (2015).
- [51] M. D. Johannes and I. I. Mazin, Fermi surface nesting and the origin of charge density waves in metals, *Phys. Rev. B* **77**, 165135 (2008).
- [52] D. S. Inosov, V. B. Zabolotnyy, D. V. Evtushinsky, A. A. Kordyuk, B. Büchner, R. Follath, H. Berger and S. V. Borisenko, Fermi surface nesting in several transition metal dichalcogenides, *New J. Phys.* **10**, 125027 (2008).
- [53] W. H. Butler, F. J. Pinski, and P. B. Allen, Phonon linewidths and electron-phonon interaction in Nb, *Phys. Rev. B* **19**, 3708 (1979).
- [54] M. Calandra and F. Mauri, Charge-density wave and superconducting dome in TiSe₂ from electron-phonon interaction, *Phys. Rev. Lett.* **106**, 196406 (2011).
- [55] F. Weber, S. Rosenkranz, J.-P. Castellan, R. Osborn, G. Karapetrov, R. Hott, R. Heid, K.-P. Bohnen, and A. Alatas, Electron-phonon coupling and the soft phonon mode in TiSe₂, *Phys. Rev. Lett.* **107**, 266401 (2011).
- [56] Y. Liu, D. F. Shao, L. J. Li, W. J. Lu, X. D. Zhu, P. Tong, R. C. Xiao, L. S. Ling, C. Y. Xi, L. Pi, H. F. Tian, H. X. Yang, J. Q. Li, W. H. Song, X. B. Zhu, and Y. P. Sun, Nature of charge density waves and superconductivity in 1T-TaSe_{2-x}Te_x, *Phys. Rev. B* **94**, 045131 (2016).
- [57] J.-G. Si, W.-J. Lu, Y.-P. Sun, P.-F. Liu, and B.-T. Wang, Charge density wave and pressure-dependent superconductivity in the kagome metal CsV₃Sb₅: A first-principles study, *Phys. Rev. B* **105**, 024517 (2022).
- [58] T. M. Rice and G. K. Scott, New mechanism for a charge density-wave instability, *Phys. Rev. Lett.* **35**, 120 (1975).
- [59] D. Jérôme, T. M. Rice, and W. Kohn, Excitonic insulator, *Phys. Rev.* **158**, 462 (1967).
- [60] A. Kogar, M. S. Rak, S. Vig, A. A. Husain, F. Flicker, Y. I. Joe, L. Venema, G. J. MacDougall, T. C. Chiang, E. Fradkin, J. van Wezel, and P. Abbamonte, Signatures of exciton condensation in a transition metal dichalcogenide, *Science* **358**, 1314 (2017).
- [61] M. Leroux, M. Le Tacon, M. Calandra, L. Cario, M.-A. Méasson, P. Diener, E. Borrisenko, A. Bosak, and P. Rodière, Anharmonic suppression of charge density waves in 2H-NbS₂, *Phys. Rev. B* **86**, 155125 (2012).
- [62] C. Heil, S. Poncé, H. Lambert, M. Schlipf, E. R. Margine, and F. Giustino, Origin of superconductivity and latent charge density wave in NbS₂, *Phys. Rev. Lett.* **119**, 087003 (2017).
- [63] T. Yildirim, Ferroelectric soft phonons, charge density wave instability, and strong electron-phonon coupling in BiS₂ layered superconductors: A first-principles study, *Phys. Rev. B* **87**, 020506(R) (2013).
- [64] X. Wan, H.-C. Ding, S. Y. Savrasov, and C.-G. Duan, Electron-phonon superconductivity near charge-density-wave instability in LaO_{0.5}F_{0.5}BiS₂: Density-functional calculations, *Phys. Rev. B* **87**, 115124 (2013).
- [65] R. Yu, Z. Fang, X. Dai, and H. Weng, Topological nodal line semimetals predicted from first-principles calculations, *Front. Phys.* **12**, 127202 (2017).
- [66] L. Fu and C. L. Kane, Topological insulators with inversion symmetry, *Phys. Rev. B* **76**, 045302 (2007).
- [67] M. Kim, C.-Z. Wang, and K.-M. Ho, Coexistence of type-II Dirac point and weak topological phase in Pt₃Sn, *Phys. Rev. B* **96**, 205107 (2017).
- [68] X.-H. Tu, P.-F. Liu, and B.-T. Wang, Topological and superconducting properties in YD₃ (D = In, Sn, Tl, Pb), *Phys. Rev. Mater.* **3**, 054202 (2019).

- [69] P. Zhang, Z. J. Wang, X. X. Wu, K. Yaji, Y. Ishida, Y. Kohama, G. Y. Dai, Y. Sun, C. Bareille, K. Kuroda, T. Kondo, K. Okazaki, K. Kindo, X. C. Wang, C. Q. Jin, J. P. Hu, R. Thomale, K. Sumida, S. L. Wu, K. Miyamoto *et al.*, Multiple topological states in iron-based superconductors, *Nat. Phys.* **15**, 41 (2019).
- [70] E. J. König and P. Coleman, Crystalline-symmetry-protected helical Majorana modes in the iron pnictides, *Phys. Rev. Lett.* **122**, 207001 (2019).
- [71] S. Qin, L. Hu, C. Le, J. Zeng, F.-C. Zhang, C. Fang, and J. Hu, Quasi-1D topological nodal vortex line phase in doped superconducting 3D Dirac semimetals, *Phys. Rev. Lett.* **123**, 027003 (2019).
- [72] X. Shi, Q. Liu, P. He, Y. Yuan, X. Kong, K. Li, and W. Zhao, Topological states in the noncentrosymmetric superconductors LaPtSi and LaPtGe, *Phys. Rev. B* **104**, 245129 (2021).
- [73] X.-B. Shi, P. He, and W.-W. Zhao, Dual topology in van der Waals-type superconductor Nb₂S₂C, *Tungsten* **5**, 357 (2023).
- [74] Y. Wu, J. Liu, and X. C. Xie, Recent progress on non-Abelian anyons: From Majorana zero modes to topological Dirac fermionic modes, *Sci. China Phys. Mech. Astron.* **66**, 267004 (2023).